JOURNAL OF MATERIALS SCIENCE 33 (1998) 2589–2594

The texture–surface morphology relationship in zinc–iron electrolytic coatings

F. CZERWINSKI*, J. A. SZPUNAR
Department of Metallurgical Engineering, McGill University, Montreal, Quebec, Canada H3A 2A7

K. KONDO
Department of Applied Chemistry, Faculty of Engineering, Okayama University, Okayama, 700 Japan
E-mail: frankcz@minmet.lan.mcgill.ca

A combination of X-ray texture measurements and atomic force microscopy topographical analysis was used to characterize the growth surface of Zn–Fe alloys electrolytically deposited on cold rolled steel substrates. Deposits, which initially exhibited a morphology of approximately 20 nm thick platelets inclined 10°–20° to the substrate surface, subsequently evolved either into triangular pyramids or hexagonal columnar crystals depending on the presence of Sn^{2+} ions in the sulphate electrolyte. The morphology of the triangular pyramids, formed in the absence of Sn^{2+} ions, had (1 0 · 0) and (0 0 · 1) planes of η (hcp) phase tilted to the substrate surface. For the morphology of hexagonal columnar crystals, formed in the presence of Sn^{2+} ions, the (0 0 · 1) basal planes of η phase were aligned parallel to the substrate surface. The macro and nano-size steps of growth were identified on both morphologies in order to locate the active growth front. It is concluded that the lateral growth on the same (0 0 · 1) basal planes of η phase led to the formation of essentially different morphologies and textures of the Zn–Fe deposits. © *1998 Chapman & Hall*

1. Introduction

Commercial production of low-carbon steel sheets, coated with zinc and zinc-based alloys for application in the automotive industry, is carried out by either hot-dipping or electroplating. For both techniques, the coatings have undergone a continuous improvement in terms of controlling their surface roughness, microstructure, coating thickness, and ability to differentiate the coating thickness on each side of the steel sheet. It is already well established that corrosion resistance, formability, weldability, and paintability are controlled by chemical composition, phase composition and microstructure [1]. According to recent findings, some of the coating properties, in particular the corrosion resistance [2] and paintability [3], are influenced by crystallographic texture. A review of the literature on this subject shows that a sharp texture develops during the hot-dip and electrodeposition of zinc and zinc alloys. While in hot-dip coatings the ⟨0 0 · 1⟩ fibre texture develops, when no alloy layer is formed on the steel surface [4], in electrolitic coatings a variety of other textures are reported [5]. It is clear, therefore, that the texture in zinc-based coatings, and its changes with manufacturing parameters, are of great practical importance.

The evolution of surface morphology and the microstructure of Zn–Fe electrodeposits as a function of zinc content and pulse current off-time were reported by Kondo *et al.* [6–11]. An interesting finding of Kondo [1] was the possibility of controlling the coating morphology by the additives of some ions to the

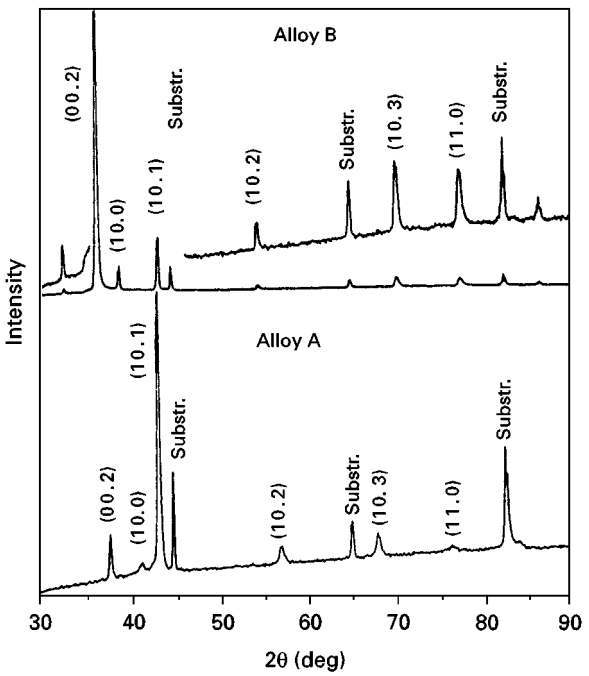

Figure 1 X-ray diffraction patterns showing the phase compositions of alloys A and B (CuK_α radiation).

* On leave from the University of Mining and Metallurgy, Cracow, Poland.

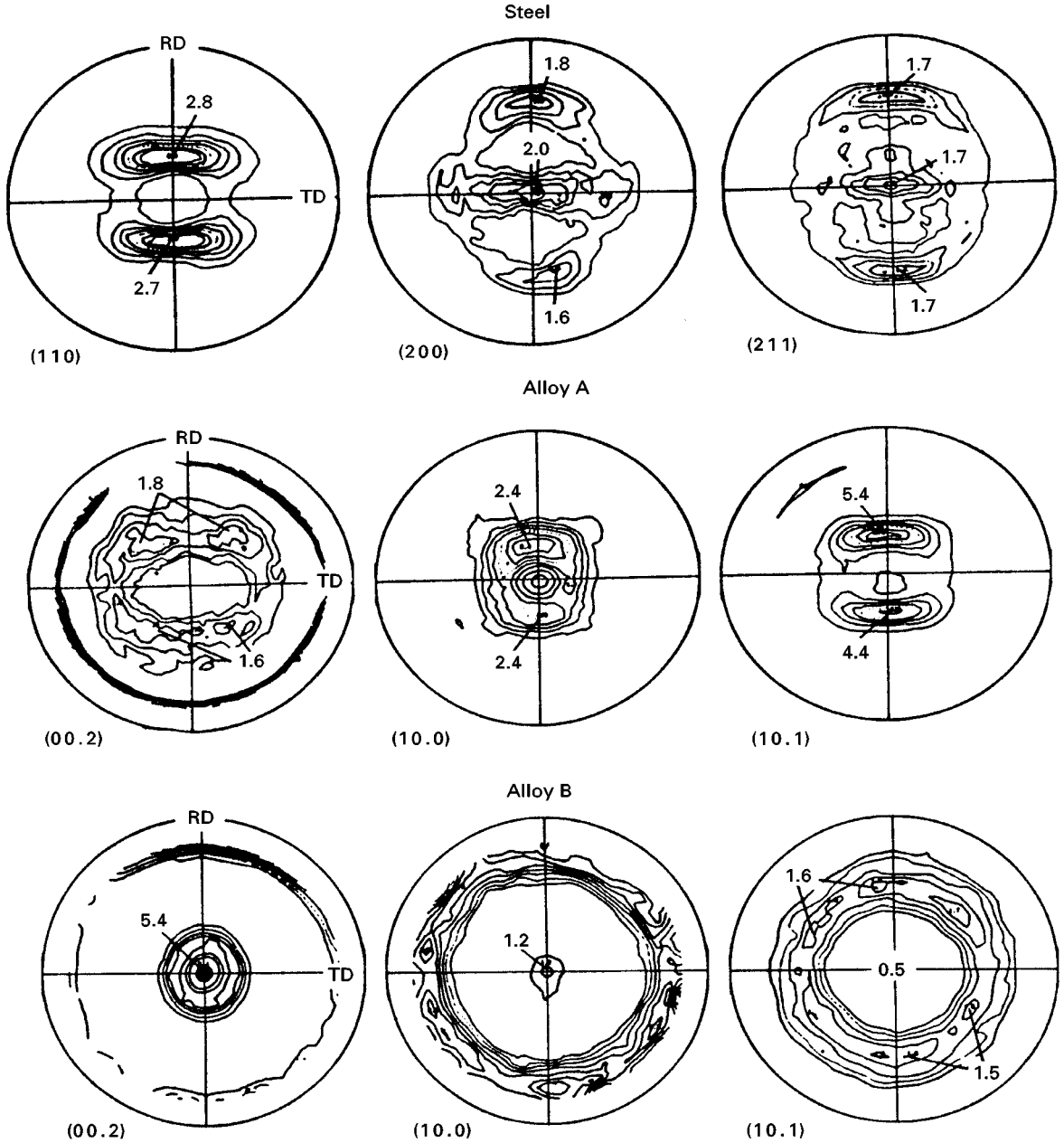

Figure 2 The selected pole figures of steel substrate and alloys A and B. Steel substrate orientation is indicated: RD, rolling direction; TD, transverse direction.

electrolyte. These additives, in fact, change the coating's textures.

In this paper we present an example of texture control in Zn–Fe coatings by Sn^{2+} additions. X-ray diffraction and atomic force microscopy (AFM) are used in order to analyse the relationship between the texture and surface topography of the coatings.

2. Experimental procedure

The electrodeposition of Zn–Fe alloys marked as A and B was conducted from an electrolyte containing: $FeSO_4$ 0.85×10^3, $ZnSO_4$ 0.76×10^3, Na_2SO_4 0.99×10^3 (mol m^{-3}). The pH of the electrolyte was kept constant at a level of 1.5, the temperature at 50 °C and the current density at a level of 8000 A m^{-2}. During the deposition of alloy B, 1 p.p.m. $SnSO_4$ was added to the electrolyte. The substrate material was a commercial low-carbon steel after cold rolling. Prior to deposition, the steel specimens were mechanically polished, degreased in acetone with an ultrasonic cleaner and etched in 10 vol % sulphuric acid.

The growth morphology of deposits was examined using the AFM technique. The AFM, a Digital Instruments Nanoscope III, was operated in contact mode using a Si_3N_4 cantilever. Three-dimensional digital images, stored in the computer's memory, were subsequently analysed by the AFM software to characterize the geometry of cross-sectional features and the parameters of surface roughness. The phase composition of alloys was derived using an X-ray Rigaku diffractometer with a rotating anode (CuK_α radiation). Texture analysis was conducted using a Siemens D-500 X-ray goniometer. Pole figures were measured using the reflection technique, tilting the specimen to a maximum of 80° in 5° intervals. The pole figures were normalized within the available interval of the distribution of crystallographic planes, and the inten-

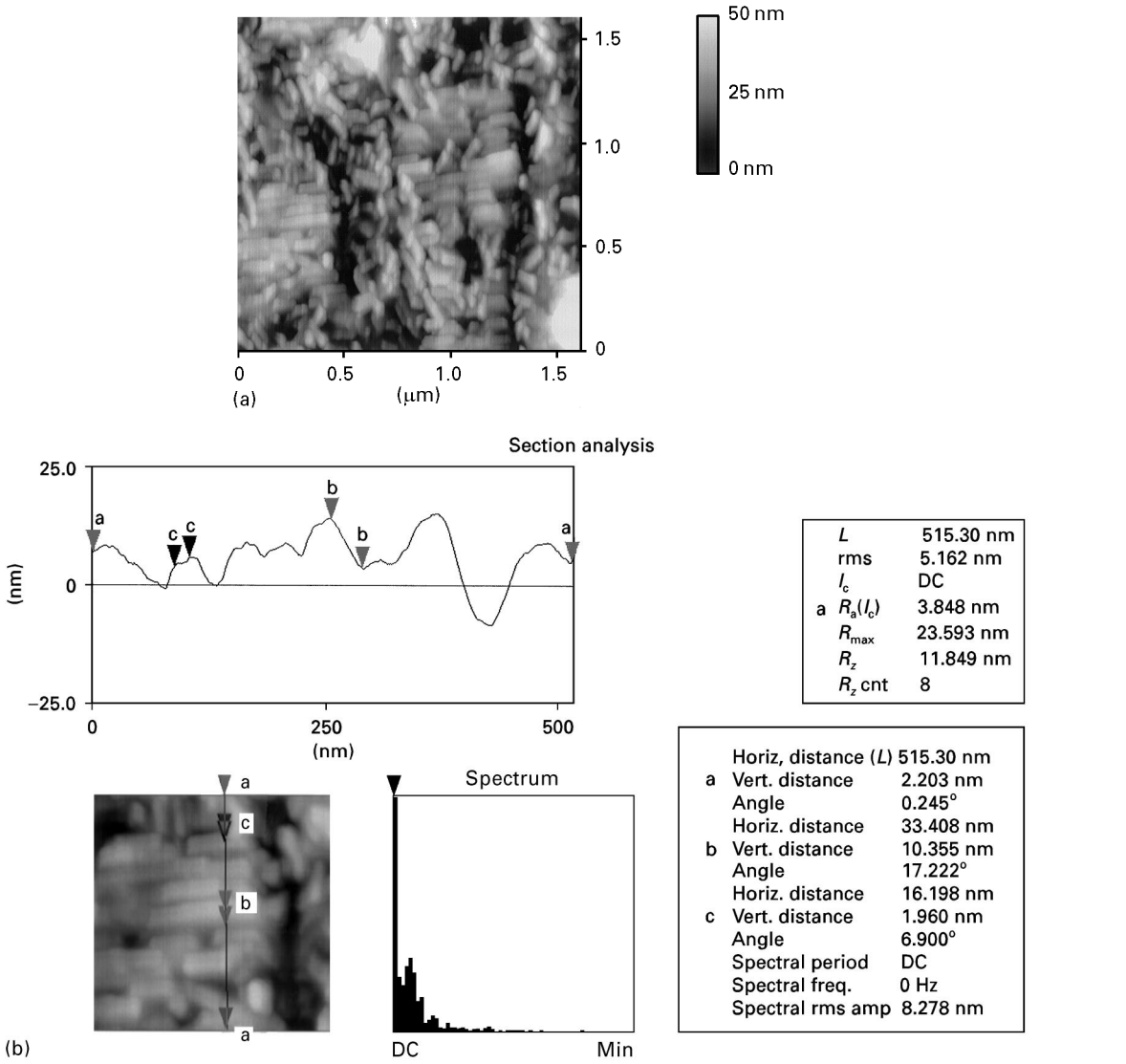

Figure 3 AFM surface morphology of Zn–Fe alloy formed during the initial stages of growth: (a) top view; (b) cross-sectional analysis of the platelets; the values of topographical parameters corresponding to the individual markers are given in the tables.

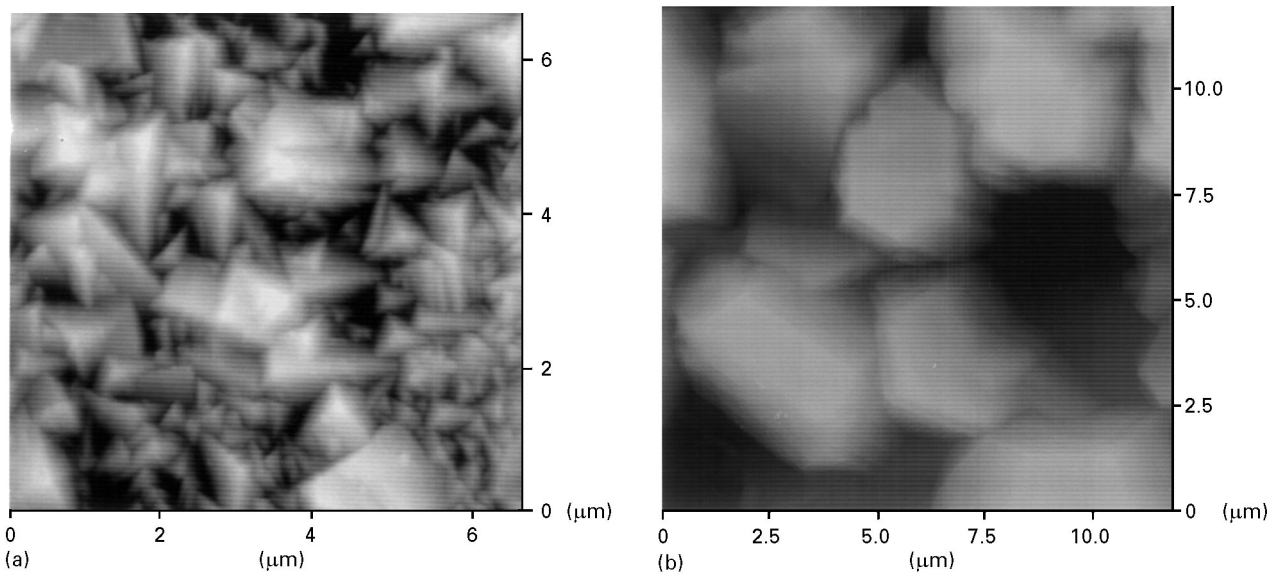

Figure 4 Top view morphology of (a) triangular pyramids and (b) hexagonal columnar crystals, imaged by AFM.

sity on the pole figures is shown using multiples of intensities from a random specimen. In order to analyse the chemical composition using inductively coupled plasma emission spectroscopy, the deposits were dissolved in 10 vol % hydrochloric acid with an inhibitor to prevent the dissolution of the steel substrate.

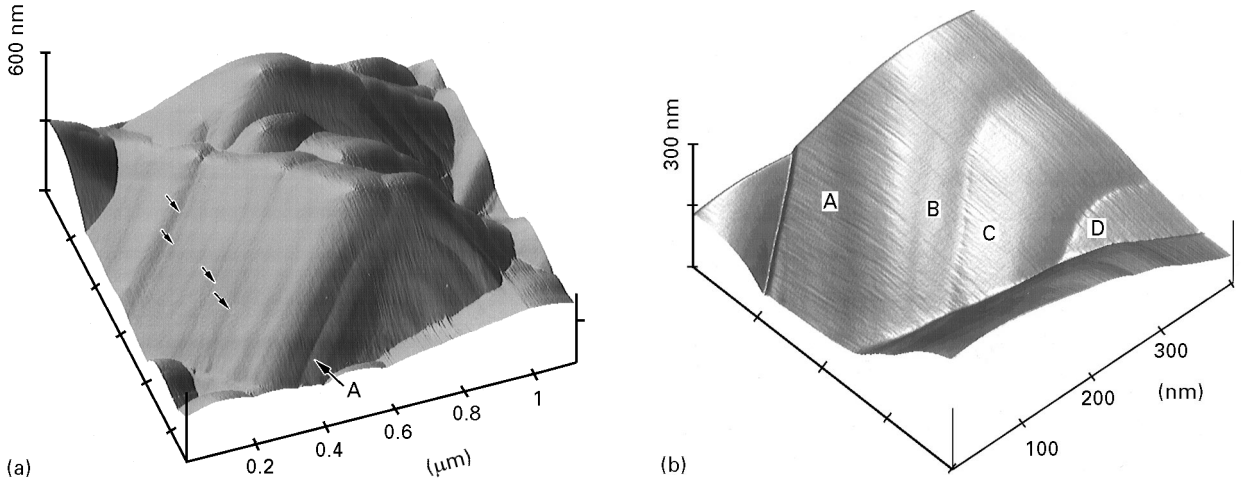

Figure 5 Analysis of the morphology of triangular pyramids: (a) three-dimensional image showing hexagonal thin platelets on the pyramid side-wall (some of the boundaries between the individual platelets are indicated by the arrows, the edge of the last, well- developed platelet is marked A; (b) high-magnification image of the platelet "A" from (a) showing that it is covered with steps of uncompleted platelets marked B, C, and D.

3. Results and discussion

3.1. Phase composition and texture

Alloys A and B, obtained under conditions of this experiment, contained 88.8 and 96.6 at % Zn, respectively, and were composed almost entirely of η phase (Fig. 1). In alloy B some traces of Γ phase in addition to the η matrix, were detected. The major difference between the X-ray diffraction patterns of both alloys was a drastic change in intensities of $(00\cdot1)$ and $(10\cdot1)$ peaks suggesting a change in crystallographic texture. In order to identify the texture components, the pole figures of selected peaks of η phase were measured.

Fig. 2a shows the texture of the steel substrate after cold rolling. A knowledge of substrate texture is of interest for the assessment of its influence on the coating texture. There is a substantial body of research indicating that, in commercial electrogalvanized steel sheets, the texture of the coatings is related to the texture of the iron substrate. According to Takechi *et al.* [2], steel sheets containing a high concentration of $\{111\}$ planes parallel to the steel surface have a $\{10\cdot3\}\langle11\cdot0\rangle$ orientation in the coating as a main one. With the decreasing concentration of $\{111\}$ planes parallel to the steel surface, the main orientation of the electroplated zinc layer changes from $\{10\cdot3\}\langle11\cdot0\rangle$ to $\{00\cdot1\}\langle uvtw\rangle$. Analysis of zinc and iron crystallography shows that by having the $\{110\}$ of iron parallel to the $\{00\cdot1\}$ plane of zinc and the $\langle111\rangle$ direction of iron parallel to the $\langle11\cdot0\rangle$ direction of zinc, the densest atomic planes and directions of both lattices nearly coincide.

The pole figures of alloy A show that the basal planes $(00\cdot1)$ of η phase are inclined about 30°–45° to the substrate surface (Fig. 2b). In addition to the fibre texture, there is also a second component with a specific crystallographic relationship between grains of Zn–Fe alloy. The latter component leads to maxima, which are marked on all three pole figures. An essentially different texture was detected in alloy B (Fig. 2c). In this case, the basal planes of η phase are aligned parallel to the substrate surface (perpendicular to the growth direction). This is expressed by $\langle00\cdot1\rangle$ fibre texture with a maximum intensity of 5.4 times random. The second texture component, a $\langle10\cdot0\rangle$ fibre with the intensity of 1.2 times random, is weak.

The comparison of pole figures for the steel substrate and the coatings shows that there is no evident correlation between the textures of the substrate and coating B. The strong $\langle00\cdot1\rangle$ fibre represents the texture developed during growth. Some influence of the substrate is seen for coating A. This is indicated by the correlation between (1 1 0) planes for substrate and $(10\cdot1)$ planes for coating. However, the fibre component with $(00\cdot1)$ basal planes of η phase inclined to the substrate surface, developed during growth and was influenced by deposition parameters.

3.2. Surface morphology

The resolution of the SEM was apparently not sufficient to distinguish the details of the morphology of the coating formed during the early stages of growth. However, the AFM revealed that, at this stage, the deposit was composed of small platelets and was relatively uniform in thickness (Fig. 3a). Although some features having heights up to 360 nm are present, the roughness of the regions between them expressed by a standard deviation root mean square (rms) [12], did not exceed 7 nm. According to the cross-sectional analysis, the platelets had thicknesses of up to 20 nm and lengths of up to 100 nm, and they were inclined 10°–20° to the substrate surface (Fig. 3b). It is believed that such a morphology was formed from fish-scale-like platelets, observed during the very initial stages and described in detail elsewhere [13]. An arrangement of platelets indicates that there was an influence of the crystallographic orientation of substrate grains, and as a result of that, the morphology changed slightly from grain to grain.

The presence of Sn^{2+} ions caused the alloys A and B to exhibit essentially different morphologies at the steady stage of growth. While the surface of alloy A, obtained from the additive-free sulphate electrolyte, showed a morphology of triangular pyramids (Fig. 4a), the surface of alloy B, formed in the presence of Sn^{2+} ions, was covered with hexagonal columnar crystals (Fig. 4b).

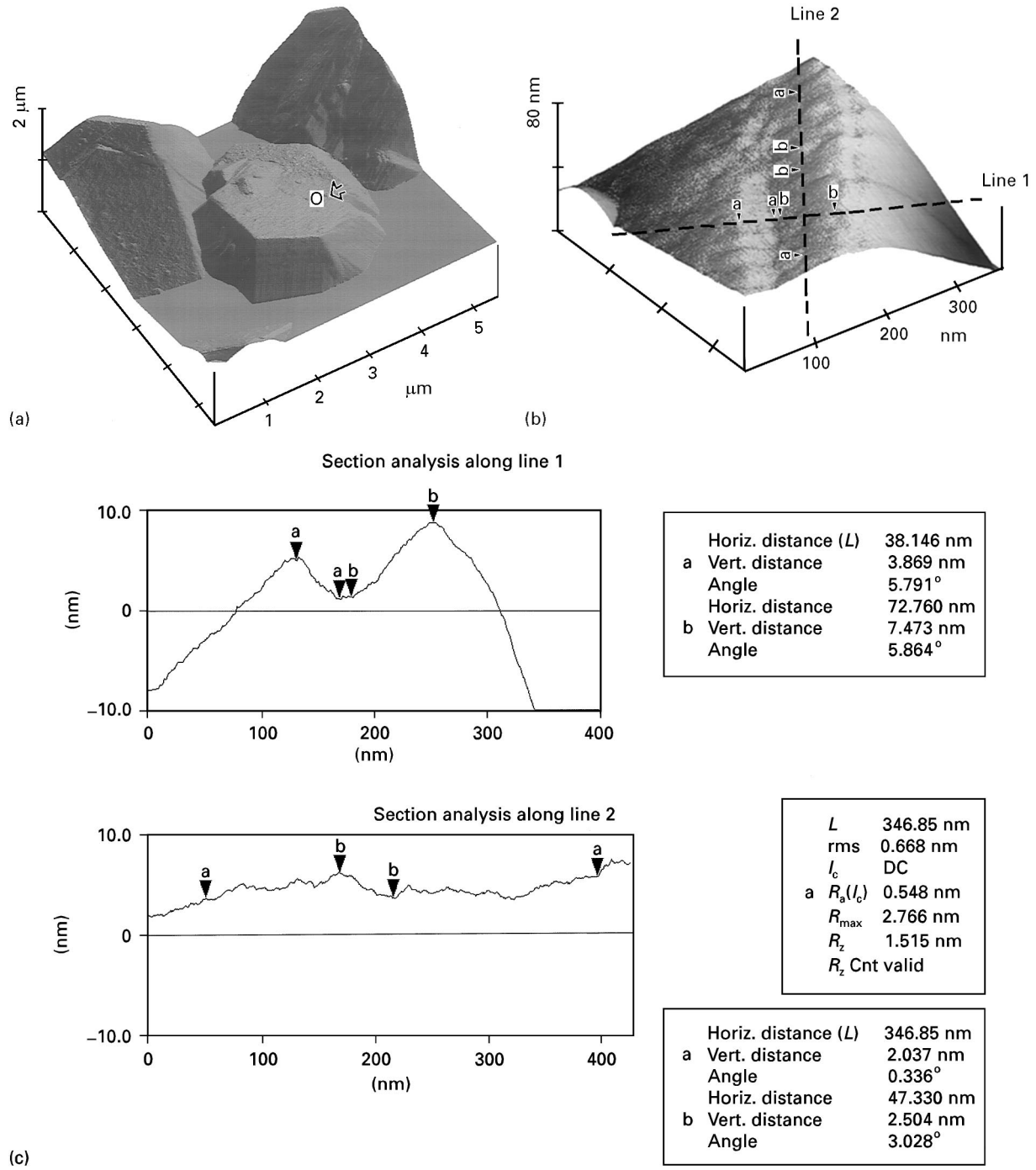

Figure 6 Analysis of the morphology of hexagonal columnar crystals: (a) three-dimensional image of the crystal; (b, c) high-magnification image of the top region of the crystal marked in (a), and the cross-sectional analysis (top surface is inclined for a better contrast): section along line "1" shows macro-steps of growth, section along line "2" shows nano-steps of growth forming the fish-scale-like pattern.

The morphology of triangular pyramids (Fig. 5a) exhibited significantly lower roughness parameters than that found for hexagonal grains. After 60 s deposition, according to AFM measurements, rms was 130 nm and maximum heights R_{max} was 715 nm. It should be emphasized that SEM images presented elsewhere [1, 6] and AFM images obtained at low magnification (Fig. 5a) are in good agreement. This finding is of special importance for AFM imaging of rough surfaces, because it is a critical indicator that no artefacts are introduced by the cantilever–surface interaction [14]. As shown in Fig. 5a, the triangular pyramids consist of side- by-side aligned thin platelets. Some of the boundaries between platelets are indicated with the arrows. A comparison of AFM topographical analysis and X-ray pole figures, supports the previous finding by Kondo [1, 7, 9] that those pyramids are surrounded by $(0\,0\cdot1)$ and $(1\,0\cdot0)$ planes of the η phase. The side-wall of the pyramid in Fig. 5a which consists of platelet with an edge labelled A, corresponds to the $(0\,0\cdot1)$ basal plane. A high-magnification image of platelet A shows that its surface contains steps of uncompleted platelets marked B, C, and D, in Fig. 5b. Thus, the lateral growth on this basal plane led to the formation of pyramidal morphology.

The deposit with a morphology of hexagonal columnar crystals was characterized by relatively high roughness parameters. For an alloy electrodeposited for 60 s, the rms roughness was 638 nm. Moreover, some individual crystals extended up to 3127 nm above the

surface. The planar size of crystals was up to 2000 nm and their shape imaged by AFM was in agreement with previous SEM observations [1, 6]. The top surfaces of the crystals were oriented parallel to the substrate surface and were covered with macro- and nano-size steps of growth (Fig. 6a). In particular, AFM revealed that nano-size steps form the fish-scale like morphology (Fig. 6b,c), very similar to that observed previously during the very early stages of the electrocrystallization of Zn-Fe alloys on the steel substrate [5, 13–18].

3.3. Growth morphology-texture relationship

The combination of crystallographic X-ray measurements and topographical AFM analysis allowed us to describe the growth surface of Zn–Fe deposits. A simple comparison of results obtained by both techniques suggests a correlation between texture and surface morphology. A strong fibre $\langle 00\cdot1\rangle$ texture is attributed to the morphology of hexagonal columnar crystals (Alloy B). This indicates that the hexagonal plates are aligned roughly parallel to the substrate surface consisting of $(00\cdot1)$ planes of η phase. The presence of steps and fish-scale-like morphology on this surface proves that the hexagonal crystals grow laterally along their $\langle 00\cdot1\rangle$ direction.

Conversely, the pole figure of alloy A with a morphology of triangular pyramids, shows that the basal plane of η phase is inclined to the substrate surface. AFM cross-sectional analysis indicates that the triangular pyramids are, in fact, hexagonal columnar crystals with basal planes inclined to the growth direction, as proposed previously [1, 6]. This implies that the pyramids are surrounded by the $(00\cdot1)$ and $(10\cdot0)$ planes of η phase. In addition, a high-magnification AFM imaging shows that these pyramids consist of the stacking of hexagonal thin plates which grow along the $\langle 00\cdot1\rangle$ direction.

It was demonstrated previously [4] that the corrosion current for zinc-coated steel in NaOH solutions is strongly affected by the coating texture. In particular, zinc grains with a near $(00\cdot1)$ orientation have much lower corrosion currents when compared with those of other orientations. The role of texture in corrosion behaviour is explained both in terms of crack initiation and metal dissolution.

Moreover, there is another aspect of texture–related behaviour. Namely, zinc-coated steel sheets are rarely used in the unpainted condition. For cosmetic appearance and for increased corrosion resistance, the steel sheets are painted before they are subjected to further processing. Leidheiser and Kim [3] showed that the paintability of zinc-coated steel sheets is greatly affected by texture. Similarly, as in the case of corrosion resistance, the zinc grains with $(00\cdot1)$ orientation parallel to the sheet surface, have better paint-adherence properties than those of other orientations. Therefore, the possibility of changing the texture and morphology of the zinc-based coatings used in this study, is of engineering importance. A $\langle 00\cdot1\rangle$ texture, formed after the addition of Sn^{2+} ions, is expected to provide a better corrosion resistance and paintability.

4. Conclusions

Electrocrystallization of Zn–Fe alloys from sulphate electrolytes, under the conditions of this experiment, starts from the form of nano-sized platelets slightly inclined to the substrate surface. During growth, this morphology evolves either to triangular pyramids or to hexagonal columnar crystals, depending on the presence of Sn^{2+} ions in the sulphate electrolyte.

The morphology of triangular pyramids, formed from an additive-free electrolyte, is accompanied by a fibre texture with $(00\cdot1)$ basal planes inclined to the substrate surface. The pyramids are composed of hexagonal platelets of η phase growing along the $\langle 00\cdot1\rangle$ direction.

The morphology of hexagonal columnar crystals, formed in the presence of Sn^{2+} ions, is accompanied by a $\langle 00\cdot1\rangle$ fibre texture. In this morphology, the basal planes are aligned parallel to the substrate surface and are covered with macro- and nano-sized steps of growth.

Acknowledgements

This research was supported by the Natural Sciences and Engineering Research Council of Canada and an ISIJ Research Promotion Grant (Japan).

References

1. K. KONDO, PhD thesis, Kyoto University (1994).
2. H. TAKECHI, M. MATSUO, K. KAWASAKI and T. TAMURA, in "Proceedings of the 6th International Conference on Texture of Materials", Vol. 2 (Iron and Steel Institute of Japan, Tokyo, 1981) p. 210.
3. H. LEIDHEISER and D. K. KIM, *J. Metals* **28** (1956) 179.
4. C.M. VLAD, M. DAHMS and H. J. BUNGE, in "Proceedings of the 8th Conference on Texture of Materials," Santa Fe, 1988 (J. S. Kallerd and G. Gottsdein (eds.), The Metalurgical Society, 1988) p. 855.
5. H. PARK, F. CZERWINSKI and J. A. SZPUNAR, *Mater. Sci. Forum* **204–206** (1996) 703.
6. K. KONDO, S. HINOTANI and Y. OHMORI, *J. Appl. Electrochem.* **18** (1988) 154.
7. K. KONDO, *ISIJ Int.* **29** (1989) 517.
8. *Idem*, *ibid.* **30** (1990) 464.
9. *Idem*, *Tetsu-to-Hagane* **74** (1988) 2300.
10. *Idem*, *ibid.* **76** (1990) 592.
11. *Idem*, *ibid.* **77** (1991) 886.
12. J.M. BENNETT and L. MATTSSON, "Surface Roughness and Scattering" (Optical Society of America, Washington, DC, 1989).
13. H. PARK, F. CZERWINSKI and J. A. SZPUNAR, in "Electrochemically Deposited Thin Films II", edited by M. Paunovic (The Electrochemical Society, Pennington, NJ, 1994) p. 146.
14. F. CZERWINSKI, K. KONDO and J. A. SZPUNAR, in "Electrochemical Synthesis and Modification of Materials", vol. 451, edited by P. Andricacos, S. G. Cocoran, J. P. Deplancke, T. P. Moffat and P. C. Searson (Materials Research Society, Pittsburgh, PA, 1997) p. 445.
15. *Idem*, *J. Electrochem. Soc.* **144** (1997) 481.
16. K. KONDO, M. YOKOYAMA and K. SHINOHARA, *J. Electrochem. Soc.* **142** (1995) 2256.
17. K. KONDO, T. MURAKAMI and K. SHINOHARA, *J. Electrochem. Soc. Lett.* **143** (1996) L75.
18. K. KONDO, T. MURAKAMI, F. CZERWINSKI and K. SHINOHARA, *ISIJ Int.* **37** (1997) 140.

Received 9 April 1997
and accepted 27 January 1998